Fully automatic segmentation of brain lacunas resulting from resective surgery using a 3D deep learning model

Raphael Fernandes Casseb[1], Brunno Machado de Campos[1], Wallace Souza Loos[3], Marcelo Eduardo Ramos Barbosa[2], Marina Koutsodontis Machado Alvim[1], Gabriel Chagas Lutfala Paulino[1], Francesco Pucci[4], Samuel Worrell[4], Roberto Medeiros de Souza[1], Lara Jehi[4], Fernando Cendes[1]

[1]Universidade Estadual de Campinas (UNICAMP), Neuroimaging Laboratory, Campinas, SP, Brazil

[2]School of Medical Sciences, Pontifical Catholic University of Campinas, Campinas, SP, Brazil

[3]Advanced Imaging and Artificial Intelligence Lab, University of Calgary, Calgary, AB, Canada

[4]Cleveland Clinic Foundation, Cleveland, OH, United States of America

Abstract

The rapid and constant development of deep learning (DL) strategies is pushing forward the quality of object segmentation in images from diverse fields of interest. In particular, these algorithms can be very helpful in delineating brain abnormalities (lesions, tumors, lacunas, etc), enabling the extraction of information such as volume and location, that can inform doctors or feed predictive models. In this study, we describe ResectVol DL, a fully automatic tool developed to segment resective lacunas in brain images of patients with epilepsy. ResectVol DL relies on the nnU-Net framework that leverages the 3D U-Net deep learning architecture. T1-weighted MRI datasets from 120 patients (57 women; 31.5 ± 15.9 years old at surgery) were used to train (n=78) and test (n=48) our tool. Manual segmentations were carried out by five different raters and were considered as ground truth for performance assessment. We compared ResectVol DL with two other fully automatic methods: ResectVol 1.1.2 and DeepResection, using the Dice similarity coefficient (DSC), Pearson's correlation coefficient, and relative difference to manual segmentation. ResectVol DL presented the highest median DSC (0.92 vs. 0.78 and 0.90), the highest correlation coefficient (0.99 vs. 0.63 and 0.94) and the lowest median relative difference (9 vs. 44 and 12 %). Overall, we demonstrate that ResectVol DL accurately segments brain lacunas, which has the potential to assist in the development of predictive models for postoperative cognitive and seizure outcomes.

1. Introduction

Epilepsy is a neurological disease with profound impacts on quality of life, morbidity and mortality. About 30 to 40% of patients do not respond to treatment with medication (Chen et al., 2018; Löscher et al., 2020) and can be referred to surgical intervention, especially if structural alterations are detected (Bernasconi et al., 2019; Duncan et al., 2016). Many factors impact surgical outcome and long-term seizure freedom is still limited, ranging from 40 to 80% (Jehi et al., 2015; Jobst & Cascino, 2015).

Studies have tried to determine the factors leading to surgical success (Fitzgerald et al., 2021; Jehi & Braun, 2021; Kuroda et al., 2021) and nomograms were created showing promising results for individualizing outcome prediction (Busch et al., 2021; Jehi et al., 2015), but there is still opportunity to increase accuracy and precision. One such untapped opportunity is fully leveraging the definition of the surgery itself. Technological advances along with big data collections enabled recent predictive models to help anticipate, for instance, cases prone to benefit from resection and what surgery approach may work best (riskcalc.org/FreedomFromSeizureRecurrenceAfterSurgery/). Chang and Englot have already pointed out that the total gross volume of the resection can be informative for predictive models (Englot & Chang, 2014) and delineation of the lacuna can help elucidate clinical changes due to function-structure relationships. However, most surgical outcome studies still capture the surgical procedure under broad categorical classifications with resolution limited to the lobe of resection (temporal/external temporal, hippocampal sparing versus resecting).

Since manual segmentation is tedious and time-consuming, initiatives to automate this task increased in the last years (Arnold et al., 2022; Billardello et al., 2022; Casseb et al., 2021). In

this study, we describe ResectVol DL, which is based on the 3D U-Net architecture using the nnU-Net framework (Isensee et al., 2020), tested on resective lacunas, and compared against two other methods: ResectVol (version 1.1.2), a rule-based method previously published by our team (Casseb et al., 2021), and DeepResection, a 2D U-Net implementation by Arnold and colleagues (Arnold et al., 2022). Our goal is to develop an open-source platform to enable surgical epilepsy research with optimal precision of the surgery definition.

2. Methods

2.1. Subjects and image datasets

Image datasets from 125 patients were retrospectively selected from the University of Campinas and the Cleveland Clinical Epilepsy Center. We included subjects with temporal (n = 45)—the most common group referred to surgery—and extratemporal lobe epilepsy (n = 75), and volunteers with no brain lesions or resective intervention (n = 5) to serve as controls for false discoveries (no-surgery data). Only resective surgeries were included.

The data that support the findings of this study are available upon reasonable request.

2.2. Manual segmentation

Five raters trained in neuroanatomy performed the manual segmentation of the surgical lacunas. Forty-eight image datasets were segmented by either two (n = 42) or three (n = 6) raters and were analyzed for inter-rater agreement.

2.3. Automatic Segmentation

To perform the automatic segmentation, we utilized ResectVol DL, which is based on the nnU-Net deep learning framework (Isensee et al., 2020). nnU-Net derives from the U-Net (Ronneberger et al., 2015), a popular deep learning architecture composed of an encoder, a decoder, and skip connections that concatenate features from the encoder to the decoder part of the network. nnU-Net is a self-configuring 3D method, meaning that it automatically determines preprocessing characteristics, architectural parameters, and post-processing features, using 3D filters. To do that, nnU-Net considers the dataset properties and computational resources, such as graphic card memory. Each processing stage of the encoding and decoding streams has two blocks of operation comprising steps of convolution, intensity normalization, and linear regularization (**Figure 1**). Data augmentation strategies include rotation, scaling, addition of Gaussian noise, Gaussian blurring, changes to brightness and contrast, simulation of low resolution, and mirroring. The model training is carried out with five cross-validation folds and 1000 epochs for each fold.

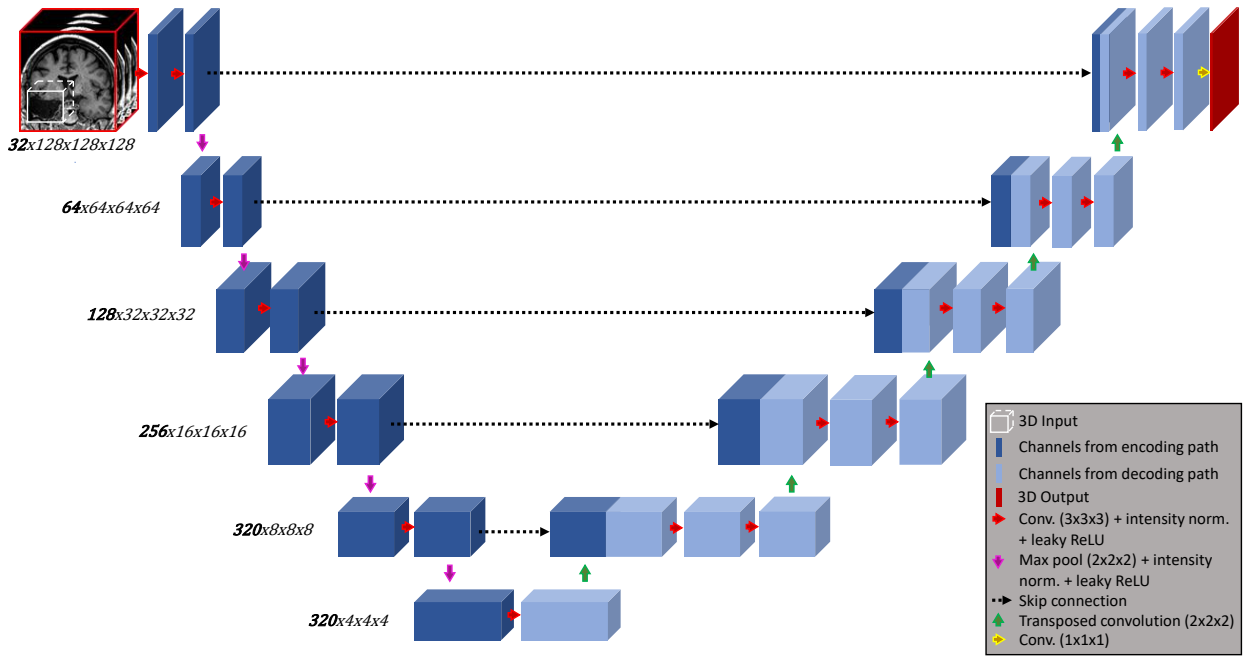

Figure 1. *Representation of the 3D nnU-Net architecture. The number of channels and resolution at each of the six stages are shown on the left (eg: there are 320 channels and a resolution of 4x4x4 in the feature map of the sixth stage). Contiguous blocks after the green arrows represent the concatenation of channels from the lower stage of the decoding branch (light blue) with channels at the same stage from the encoding branch (dark blue).*

To compare our algorithm against other freely available tools, we also performed the lacuna prediction with two other approaches: ResectVol version 1.1.2 (freely available at lniunicamp.com/resectvol), a rule-based algorithm developed by our group (Casseb et al., 2021); and the DeepResection tool (available at github.com/penn-cnt/DeepResection) developed by Arnold and colleagues (Arnold et al., 2022) that uses a set of three 2D U-Nets, each in one anatomical plane, followed by voxel-wise majority voting. In ResectVol 1.1.2, it is mandatory for users to provide the pre- and postoperative images to run the analysis, whereas in DeepResection, users are required to provide the postoperative image only.

2.4. Computational Resources

All automatic processing was performed on a 3.6 GHz Intel(R) Core(TM) i7-12700KF CPU with 32-GB RAM, a 48-GB NVIDIA RTX A6000, and a 20.04.1 Ubuntu operational system.

2.5. Performance Assessment

The Dice similarity coefficient (DSC) (Dice, 1945) was used as an indirect measure of overlap between manual and automatic segmentations, ranging from 0 (no overlap) to 1 (perfect overlap). In the imaging domain, DSC can be interpreted as the ratio between the number of

intersecting voxels of two spatial volumes, say V_A and V_B, and the sum of the number of voxels in each volume, yielding the equation:

$$DSC = \frac{2 \times |V_A \cap V_B|}{V_A + V_B},$$

where the factor 2 is used to normalize DSC to the [0,1] interval.

We also calculated the volume obtained from the manual and the automatic segmentations and estimated Pearson's correlation and the volume difference percentage between them (the relative difference, using the manual volume as reference).

Additionally, to investigate if there were differences associated with lacuna size, we split lacunas into two groups (large and small) based on their median volume and compared the DSCs.

Regarding the inter-rater performance, we calculated the DSC for the 48 images that were manually segmented more than once.

This study was conducted with approval from the Cleveland Clinical Foundation Institutional Review Board. Informed consent was waived due to the retrospective nature of the data collection. All images used in this study were anonymized.

3. Results

3.1. Subjects

One hundred and twenty patient volunteers (57 women; 31.5 ± 15.9 years old at surgery) had temporal (n = 45; 23 women; 37.7 ± 13.8 years old) and extratemporal (n = 75; 34 women; 27.8 ± 16.0 years old) epilepsy, whereas five subjects (2 women; 29.0 ± 4.5 years old) were included as controls who were not submitted to any brain surgery. Nearly all postoperative images were acquired 5 months (median: 6.2; Q1 - Q3: 6.0 - 8.0; range: .2 - 63.9) after surgery, to avoid necrotic tissue that could be misleading in the segmentation process. Seventy-three patients were seizure-free (Engel Ia) after surgery.

3.2. Imaging protocol

T1 weighted anatomical MR images were obtained in eight different MRI systems (1.5 and 3 T) from two different vendors (Siemens and Philips). Acquisition parameters and image quality varied, benefiting the robustness of the performance assessment since datasets posed a diverse scenario in which to try the tested tools. Parameters can be summarized in the following ranges: voxel size = 0.41 × 0.45 × 0.41 to 1 × 2 × 1 mm^3; TR = 7 to 2200 ms; TE = 2.3 to 46 ms; and image matrix = 180 x 96 to 512 x 512.

3.3. Manual segmentation

All the images containing brain lacunas (n = 120) were manually segmented at least once. Three of the five raters timed the duration of manual delineation in a subset of images and obtained the approximated median times: 114 min (MERB, n = 31); 70 min (RFC, n = 14); 54 min (GCLP, n = 19). Forty-eight images were segmented by two different raters at least, and the median DSC was .88 (Q1 - Q3: .78 - .91; range: .00 - .97). We visually selected the best manual mask in these cases to compose the final set of 120 manual masks used in the subsequent analyses.

3.2. ResectVol DL

Seventy-two images were used to train the nnU-Net architecture which lasted 77 hours and 17 minutes. In summary, the final configuration of the network encompasses two streams – an encoder and a decoder – with six resolution stages. **Figure 1** shows a schematic representation of the 3D nnU-Net model deployed in this study.

We found a median DSC of .92 (.88 - .94) and .91 (Q1 - Q3: .86 - .94) for the test and the cross-validation set, respectively (**Table 1**).

For 47 of the 48 test images, ResectVol DL was able to correctly identify the lacuna (DSC ≥ .612) and it failed for only one extratemporal case – the smallest lacuna in the sample. The correlation between the manual and the automatic volumes was $r(46) = .99$ ($p < .001$), with a median relative difference of 9 % (Q1 - Q3: 4 - 15 %). ResectVol DL correctly identified the absence of lacunas in the five false positive datasets. The prediction for each image took, on average, 41.7 seconds. As the available version of DeepResection is only intended for temporal resections, we report correlation and median relative difference for temporal, extra-temporal, and all data in **Table 1**. In **Figure 2**, we show the scatter plots for all data (**Figure 2A**), and also for temporal cases in **Figure 2B-D**, along with the corresponding linear fit.

3.3. Performance of other approaches

The test set of 53 images (48 lacunas and five no-surgery controls) was also processed by ResectVol 1.1.2 and DeepResection.

ResectVol 1.1.2 requires no pre-processing of the images but requires both pre-and postoperative images to calculate the lacuna volumes, while ResectVol DL requires only the postoperative images. It took on average 9 minutes and 17 seconds to process each dataset composed of the pre- and the postoperative images. We found a median DSC = .78 (Q1 - Q3: .65 - .84), a correlation between the manual and automatic volumes of $r(46) = .63$ ($p < .001$), and a median relative difference of 44 % (Q1 - Q3: 29 – 75 %). For the five control images, it incorrectly found lacuna in all five cases (volume range: .3 - 4.2 cm^3).

Similar to both versions of ResectVol, DeepResection does not require any preprocessing. The authors do recommend, however, that images are in Left-Anterior-Superior orientation because predictions can be inaccurate otherwise. We used *fslorient* function from the FMRIB Software Library (FSL) (Jenkinson et al., 2012) to perform the reorientation. Predictions of temporal

lacunas (extratemporal excluded) overlapped with the manual segmentation in all cases, yielding a DSC = .90 (.86 - .92). Median correlation and relative difference were r(46) = .94 (p < .001) and 12 % (Q1 - Q3: 6 – 20 %), respectively. **Figure 3** exhibits the best, median, and worst DSC-associated cases for all tools.

Table 1. *Dice Similarity Coefficient (DSC), correlation, and relative difference obtained with each method for the test set*

		ResectVol DL	***ResectVol 1.1.2***	***DeepResection***
All data	**median DSC (Q1 - Q3)**	***.92 (.88 - .94)***	.78 (.65 - .84)	.07 (0 - .89)*
	Range	0 - .96	0 - .90	0 - .95*
	correlation (p-val)	.99 (< .001)	.63 (< .001)	----
	median rel. diff. (Q1 - Q3)	9 (4 - 15) %	44 (29 - 75) %	----
Temporal	**median DSC (Q1 - Q3)**	***.93 (.89 - .95)***	.79 (.75 - .86)	.90 (.86 - .92)
	Range	.85 - .96	.21 - .90	.20 - .95
	correlation (p-val)	.97 (< .001)	.72 (<.001)	.94 (< .001)
	median rel. diff. (Q1 - Q3)	8 (4 - 11) %	45 (30 - 65) %	12 (6 - 20) %
Extra-temporal	**median DSC (Q1 - Q3)**	**.92 (.88 - .94)**	.73 (.61 - .79)	0 (0 - 0)*
	Range	0 - .96	0 - .89	0 - .08*
	correlation (p-val)	.99 (< .001)	.62 (.001)	----
	median rel. diff. (Q1 - Q3)	10 (4 - 20) %	37 (15 - 84) %	----
No-surgery data	**5 cases**	***0***	5	***0***

* *DeepResection* authors do not recommend applying it to extra-temporal cases. These values are just reported for completeness. The associated correlation values, however, are not displayed due to the impossibility related to data distribution (see **Figure 2A**, bottom plot).

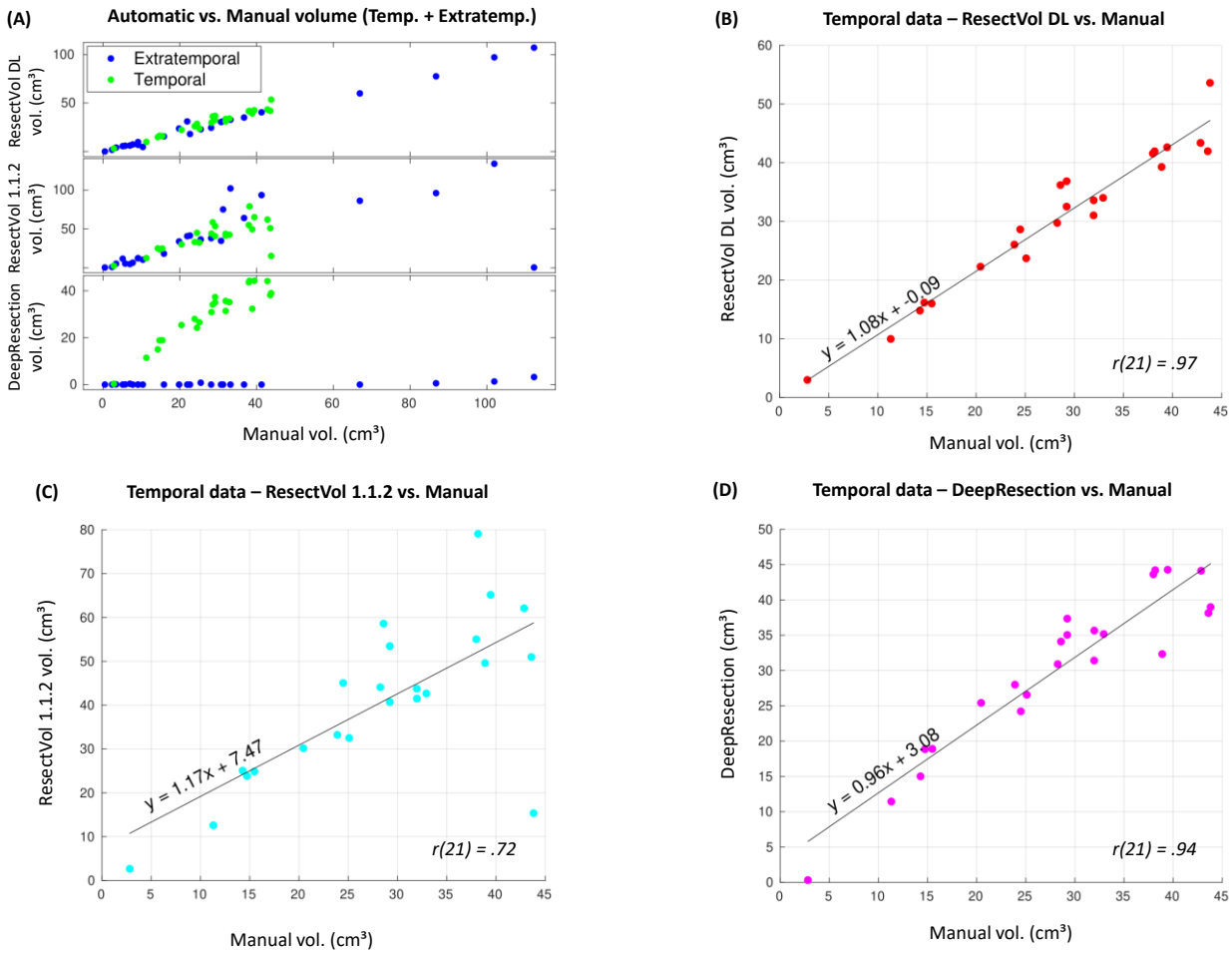

Figure 2. *(A) Scatter plots for all data (temporal + extratemporal cases) (A) and for temporal data only (B-D) (between each segmentation method and manual delineation). Plots B-D include the linear fit, the equation that best adjusts to the data, and the correlation value r.*

3.4. Large vs. small lacunas

The Spearman's correlation between volume (in cm³) and DSCs was r_s (46) = .60 ($p < .001$). To further assess this significant relationship, we ranked lacunas by their size obtained with the manual delineation and split our dataset into two subgroups based on the median lacuna volume (25.5 cm³). We investigated whether there was any difference in DSC across the small (< 25.5 cm³) and the large lacunas (> 25.5 cm³) (**Figure 4**). Since the data in each group was not normally distributed, we performed non-parametric tests to compare groups. The Mann-Whitney U test revealed a significant difference between groups (U = 450.5, p = .001).

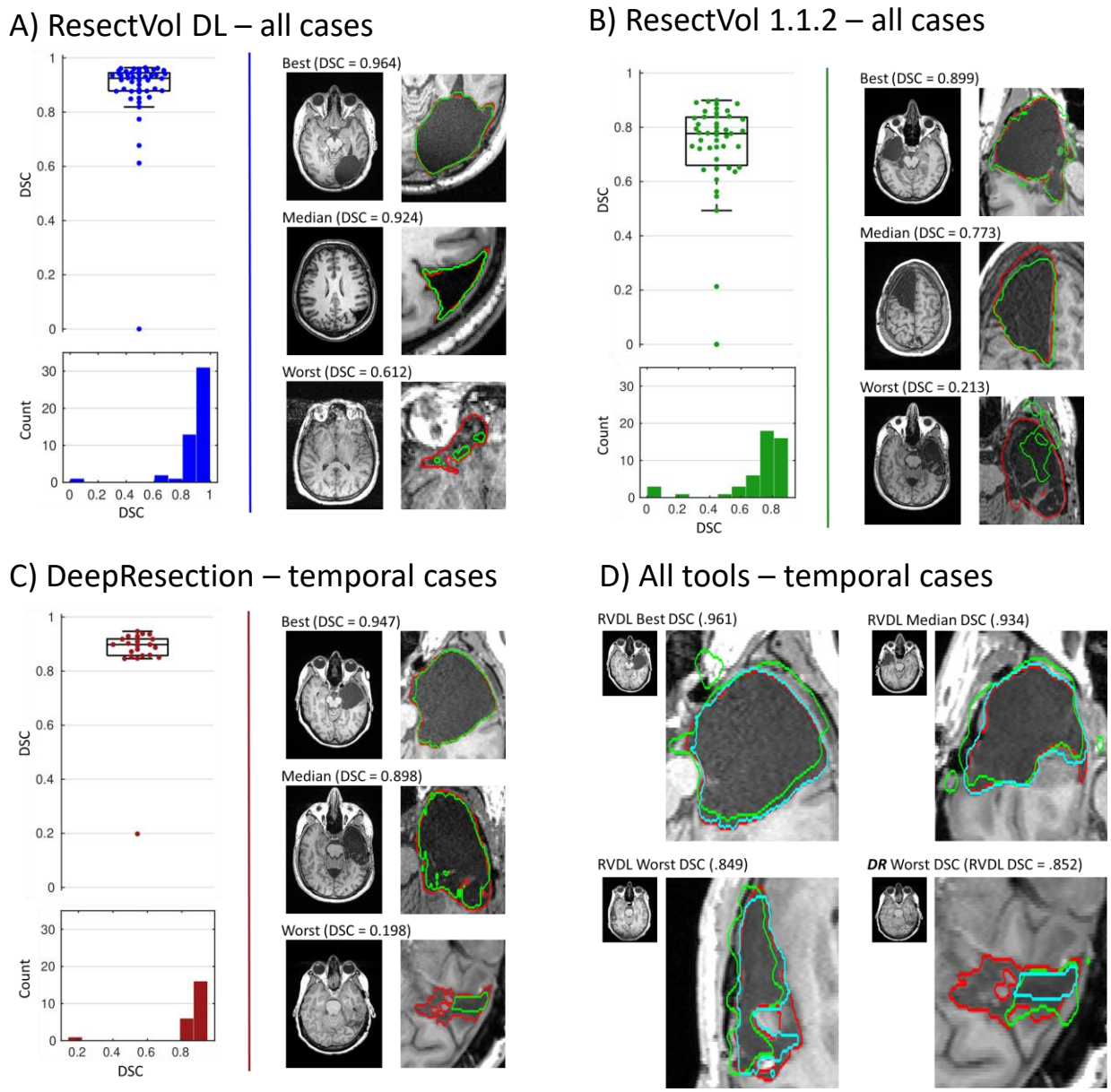

Figure 3. *Boxplots, histograms, and noteworthy cases for (**A**) ResectVol DL (RV2), (**B**) ResectVol 1.1.2 (RV112), and (**C**) DeepResection (DR), along with Dice similarity coefficient (DSC). Red and green contours in **A-C** represent manual and automatic segmentation. Both versions of ResectVol (**A** and **B**) were applied to temporal and extratemporal data (n = 48), whereas DeepResection (**C**) is only applied to temporal cases (n = 23) due to its limitation. In **D** we display contours obtained with RVDL (red), RV112 (green), and DR (cyan) in temporal cases (to allow visual comparison across the three tools). Although included in boxplots and histograms, cases with DSC = 0 are not shown in the figures.*

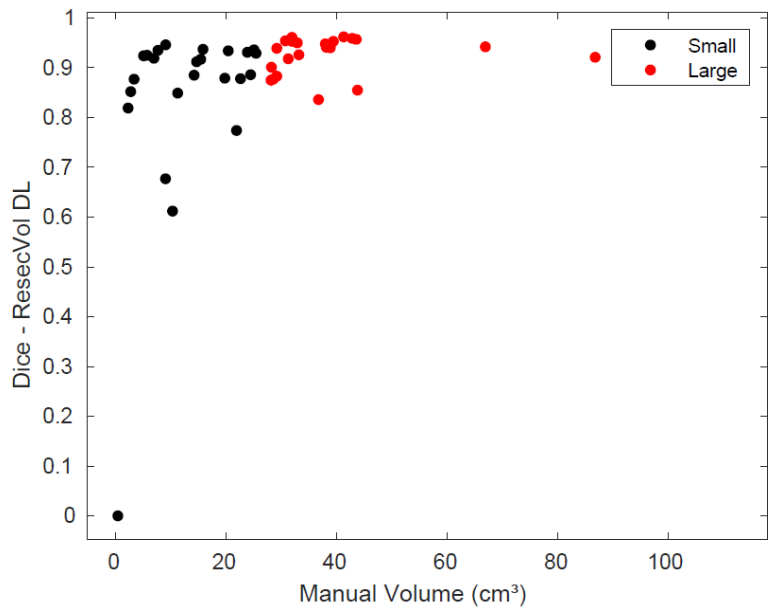

Figure 4. *Distribution of Dice similarity coefficients (DSC) as a function of lacuna volume. Small lacunas (red dots) show more diverse values of DSC than large ones (black dots).*

3.5. Structure identification

After segmenting the lacuna, ResectVol DL combines the lacuna mask with the brain-extracted image to estimate the original 3D brain shape. This recreated whole brain undergoes a series of registration steps that registers a labeled template in the Montreal Neurological Institute (MNI) space onto the space of the original image (native). We use the Desikan-Killiany-Tourville (DKT) atlas (Klein & Tourville, 2012) as a reference for naming brain structures. Our pipeline uses functions from the Advanced Normalization Tools (ANTs) (Avants et al., 2011) package, the Statistical Parametric Mapping (SPM) (Friston et al., 1994) toolbox, and FSL. **Figure 5** illustrates an example of the labeled regions in a temporal patient along with the table containing the volumetric information.

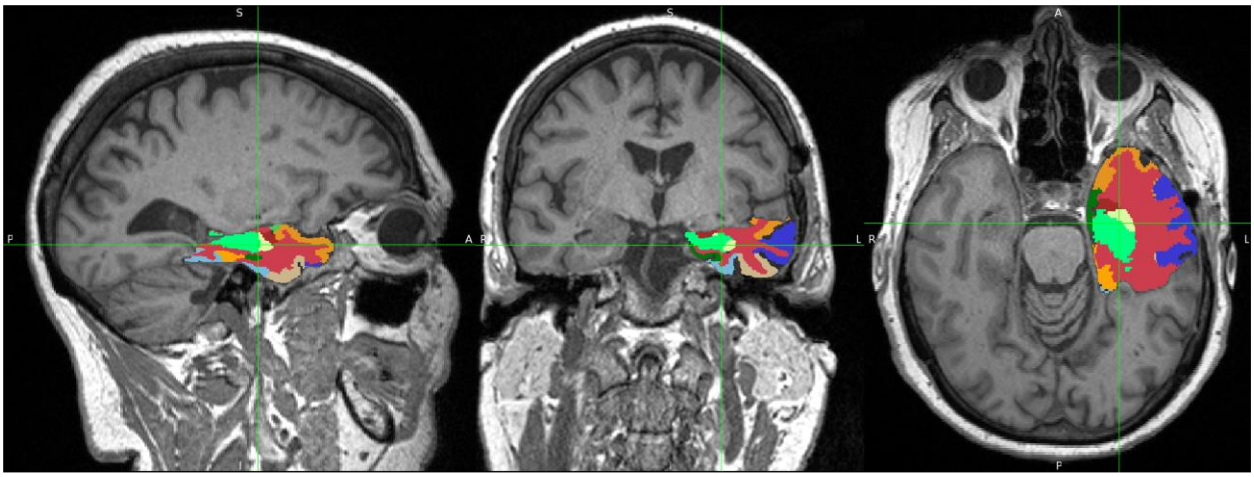

Cluster 1:				
Volume: 253376 voxels (42624.98 mm3)				
ROI Index	**ROI Name***	**Resected vol (voxel)**	**Resected vol (mm3)**	**Resected %**
1006	ctx-lh-entorhinal	6205	1043.86	80
17	Left-Hippocampus	14909	2508.11	71
18	Left-Amygdala	4255	715.81	69
1016	ctx-lh-parahippocampal	3061	514.95	44
1009	ctx-lh-inferiortemporal	27193	4574.63	43
1015	ctx-lh-middletemporal	29366	4940.19	38
1030	ctx-lh-superiortemporal	32002	5383.64	34
1007	ctx-lh-fusiform	7822	1315.88	21
2	Left-Cerebral-White-Matter	102551	17251.96	7
999	Undetermined**	25213	4241.54	---

Figure 5. *Region labeling in the lacuna segmentation (top) and the corresponding volumetric information table (bottom).*

4. Discussion

In this study, we compared 3 different segmenting methods against the manual delineation of brain lacunas in T1-weighted MR images. We found that ResectVol DL, which relies on the nnU-Net architecture, could outperform our previous rule-based implementation (version 1.1.2), and another deep learning method, DeepResection, based on the 2D U-Net architecture. To the best of our knowledge, DeepResetion, ResectVol 1.1.2, and ResectVol DL are the only freely available, fully automatic tools dedicated to this task.

Lacuna segmentation is a valuable procedure in the epilepsy field because it can offer a means of estimating characteristics of the removed brain region and informing predictive models of surgery outcome. Manual segmentation is the obvious first approach considered, and arguably the one with the best quality, but it is susceptible to human error and consistency factors, such as inter and intra-rater variability. A subset of images from our study (n = 48) were segmented

by two (or more) raters to estimate the inter-rater DSC. When more than two segmentations were available, we chose the highest DSC among the ones obtained, yielding a more human-favorable estimate to be compared against the automatic methods. We found an inter-rater DSC of .88.

Raters spent more time performing manual segmentation in our study (approximately or more than 1 hour) than what has been reported by other authors (approximately 30 minutes) (Casseb et al., 2021; Gau et al., 2020). We found that duration depends on lesion complexity (as reported in these studies), tool used, and rater experience. Computer systems can spare humans from these repetitive tasks and accelerate their completion, besides avoiding the mentioned human error and variability.

In line with that, semi-automated methods have been implemented in which users need to click on a point inside the lacuna to carry out the segmentation. Gau et al. (Gau et al., 2020), for instance, employed itk-SNAP segmenting software (www.itksnap.org) (Yushkevich et al., 2006) to perform the lacuna delineation by manually setting a seed inside the lacuna, followed by the itk-SNAP's region-growing algorithm, and found a median DSC = .78 (range: .53 - .94). More recently, Billardello and colleagues (Billardello et al., 2022) created a tool that also requires the user to click on (or set the coordinates of) a voxel to be used as the seed for the region-growing algorithm. In their graphical interface, users can also set parameters to optimize the process and choose the desired outputs. They found a median DSC = .83 (Q1 - Q3: .72 - .85). The major advantage of these approaches is that the seed is always positioned in the right location where the lacuna is expected to be identified, practically eliminating the false negative result (i.e., not finding a lacuna when there is one) or mislocating the lacuna. Nevertheless, this approach still demands human intervention, is prone to bias – since manual positioning of the seed may lead to different results –, and, although we did not do a direct comparison on the same dataset, the DSC found for ResectVol DL in the present study (.93) is better than in the previous studies.

Among the fully automatic tools we tested, DeepResection was the fastest (~35 s per image), ResectVol DL was second (~42 s), whereas ResectVol 1.1.2 took much longer (~9 min) due to the nature of its processing algorithm which is based on a series of processing steps. However, when comparing median DSCs for temporal cases, ResectVol DL was the best one (DSC = .93) followed by DeepResection (.90) and ResectVol 1.1.2 (.79). Although DeepResection is capable of being fine-tuned to work with extratemporal resections – as tested in the original publication (exploratory DSC = .75) - authors do not recommend using this preliminary fine-tuned model. Hence, for extratemporal cases, we only considered the results from both versions of ResectVol, and, again, version DL was the winner (.92 vs .73). ResectVol DL only failed in one extra-temporal case, whereas ResectVol 1.1.2 failed in two cases. None of the fully automatic tools failed in temporal resections. Regarding the control images, ResectVol DL and DeepResection did not produce any false positive results in the five control images. ResectVol 1.1.2 found false positive results in the five control datasets.

As previously reported in other studies (Arnold et al., 2022; Gau et al., 2020), we found a relationship between DSC and lacuna size indicating that there is a trend towards better performance for larger resection. Since DSC is dependent upon a volume ratio, large values in the numerator (intersection) and denominator (total volume) will be less sensitive to intersection mismatches when comparing two volumetric shapes. Hence, small lacunas are more prone to be affected by discrepancies and present more variability in DSCs (**Figure 4**).

Besides the volumetric information obtained with such computational segmentation methods, this line of research may offer potential avenues for surgery planning and outcome prediction. Koepp et al. showed that the removal of at least 50% of the piriform cortex increased (by a factor of 16) the odds of becoming seizure-free, and no relationship was found with other mesiotemporal structures (e.g.: hippocampus, amygdala, and entorhinal cortex) (Koepp et al., 2019). Leon-Rojas and colleagues implemented a pipeline, based on this result and on their dataset of resective surgeries, to automatically segment the piriform cortex and calculate chances of seizure freedom during planning (Leon-Rojas et al., 2021). They were able to plan a new patient intervention with an estimated 50% chance of long-term seizure freedom. At the 12-month follow-up, the patient presented with no seizures or auras. The automatic segmentation of resected areas can help increase knowledge and accelerate the development of such tools. Since ResectVol can list areas removed along with their volume, it can also help serve that purpose.

Regarding the inter-rater assessment, we found a DSC = .88, comparable to previous reports on brain tumors (.84 - .86) (Ermiş et al., 2020) and lacuna resection (.84) (Pérez-García et al., 2020). We noticed idiosyncrasies among raters, that were more pronounced in temporal resections, especially in the very medial region near the hippocampus. We do recommend that researchers carefully check, or standardize—if possible—, important resection areas if they anticipate that some regions may be controversial.

Limitations of our tool include not being tested on postoperative MRIs of other surgery types, like laser interstitial thermal therapy. However, we anticipate that, due to the different profiles of lesioned brain sites, a new network should be trained on this specific dataset to accommodate these discordant characteristics. We also have not validated the labeling of resected brain structures, which is an area that does deserve attention in future studies. Overall, ResectVol DL had the best performance across the tested tools, having failed for only one case out of 53 on which it was tested. It can be utilized in temporal and extratemporal cases and is freely available at (github.com/rfcasseb/resectvol_dl/).

5. Conclusion

The latest update of ResectVol (version DL) successfully segmented brain lacunas in MRIs of patients with epilepsy who have undergone surgery. ResectVol DL is fast, accurate, and does not require any image pre-processing. It relies solely on postoperative images to measure lacuna volumes. ResectVol DL also provides estimates of the volumes of various anatomical

structures within the lacuna. This enables more precise estimation of volumetric information, which facilitates additional studies such as fMRI investigations performed prior to surgery. Moreover, it may aid in generating predictive models of surgical results.

6. Acknowledgements

This work was supported by the São Paulo Research Foundation (2020/00019-7 and 2013/07559-3) and the National Institutes of Health (R01NS097719).

7. References

Arnold, T. C., Muthukrishnan, R., Pattnaik, A. R., Sinha, N., Gibson, A., Gonzalez, H., Das, S. R., Litt, B., Englot, D. J., Morgan, V. L., Davis, K. A., & Stein, J. M. (2022). Deep learning-based automated segmentation of resection cavities on postsurgical epilepsy MRI. *NeuroImage : Clinical*, *36*, 103154. https://doi.org/10.1016/J.NICL.2022.103154

Bernasconi, A., Cendes, F., Theodore, W. H., Gill, R. S., Koepp, M. J., Hogan, R. E., Jackson, G. D., Federico, P., Labate, A., Vaudano, A. E., Blümcke, I., Ryvlin, P., & Bernasconi, N. (2019). Recommendations for the use of structural magnetic resonance imaging in the care of patients with epilepsy: A consensus report from the International League Against Epilepsy Neuroimaging Task Force. *Epilepsia*, *60*(6). https://doi.org/10.1111/epi.15612

Billardello, R., Ntolkeras, G., Chericoni, A., Madsen, J. R., Papadelis, C., Pearl, P. L., Grant, P. E., Taffoni, F., & Tamilia, E. (2022). Novel User-Friendly Application for MRI Segmentation of Brain Resection following Epilepsy Surgery. *Diagnostics 2022, Vol. 12, Page 1017*, *12*(4), 1017. https://doi.org/10.3390/DIAGNOSTICS12041017

Busch, R. M., Hogue, O., Miller, M., Ferguson, L., Mcandrews, M. P., Hamberger, M., Kim, M., Mcdonald, C. R., Reyes, A., Drane, D. L., Hermann, B. P., Bingaman, W., Najm, I. M., Kattan, M. W., & Jehi, L. (2021). Nomograms to Predict Verbal Memory Decline After Temporal Lobe Resection in Adults With Epilepsy. *Neurology*, *97*(3). https://doi.org/10.1212/WNL.0000000000012221

Casseb, R. F., de Campos, B. M., Morita-Sherman, M., Morsi, A., Kondylis, E., Bingaman, W. E., Jones, S. E., Jehi, L., & Cendes, F. (2021). ResectVol: A tool to automatically segment and characterize lacunas in brain images. *Epilepsia Open*, *6*(4), 720–726. https://doi.org/10.1002/EPI4.12546

Chen, Z., Brodie, M. J., Liew, D., & Kwan, P. (2018). Treatment outcomes in patients with newly diagnosed epilepsy treated with established and new antiepileptic drugs a 30-year longitudinal cohort study. *JAMA Neurology*, *75*(3). https://doi.org/10.1001/jamaneurol.2017.3949

Dice, L. R. (1945). Measures of the Amount of Ecologic Association Between Species. *Ecology*, *26*(3), 297–302. https://doi.org/10.2307/1932409

Duncan, J. S., Winston, G. P., Koepp, M. J., & Ourselin, S. (2016). Brain imaging in the assessment for epilepsy surgery. In *The Lancet Neurology* (Vol. 15, Issue 4). https://doi.org/10.1016/S1474-4422(15)00383-X

Englot, D. J., & Chang, E. F. (2014). Rates and predictors of seizure freedom in resective epilepsy surgery: An update. In *Neurosurgical Review* (Vol. 37, Issue 3, pp. 389–405). Springer Verlag. https://doi.org/10.1007/s10143-014-0527-9

Ermiş, E., Jungo, A., Poel, R., Blatti-Moreno, M., Meier, R., Knecht, U., Aebersold, D. M., Fix, M. K., Manser, P., Reyes, M., & Herrmann, E. (2020). Fully automated brain resection cavity delineation for radiation target volume definition in glioblastoma patients using deep learning. *Radiation Oncology*, *15*(1). https://doi.org/10.1186/s13014-020-01553-z

Fitzgerald, Z., Morita-Sherman, M., Hogue, O., Joseph, B., Alvim, M. K. M., Yasuda, C. L., Vegh, D., Nair, D., Burgess, R., Bingaman, W., Najm, I., Kattan, M. W., Blumcke, I., Worrell, G., Brinkmann, B. H., Cendes, F., & Jehi, L. (2021). Improving the prediction of epilepsy surgery outcomes using basic scalp EEG findings. *Epilepsia*, *62*(10). https://doi.org/10.1111/epi.17024

Gau, K., Schmidt, C. S. M., Urbach, H., Zentner, J., Schulze-Bonhage, A., Kaller, C. P., & Foit, N. A. (2020). Accuracy and practical aspects of semi- and fully automatic segmentation methods for resected brain areas. *Neuroradiology*, *62*(12), 1637–1648. https://doi.org/10.1007/s00234-020-02481-1

Isensee, F., Jaeger, P. F., Kohl, S. A. A., Petersen, J., & Maier-Hein, K. H. (2020). nnU-Net: a self-configuring method for deep learning-based biomedical image segmentation. *Nature Methods 2020 18:2*, *18*(2), 203–211. https://doi.org/10.1038/s41592-020-01008-z

Jehi, L., & Braun, K. (2021). Does etiology really matter for epilepsy surgery outcome? *Brain Pathology*, *31*(4). https://doi.org/10.1111/bpa.12965

Jehi, L., Yardi, R., Gonzalez-Martinez, J., Chagin, K., Kattan, M. W., Bartolomei, F., Jehi, L., Yardi, R., Chagin, K., Tassi, L., Russo, G. Lo, Worrell, G., Hu, W., Cendes, F., Morita, M., Bartolomei, F., Chauvel, P., Najm, I., Gonzalez-Martinez, J., … Kattan, M. W. (2015). Development and validation of nomograms to provide individualised predictions of seizure outcomes after epilepsy surgery: a retrospective analysis. *Articles Lancet Neurol*, *14*, 283–290. https://doi.org/10.1016/S1474-4422(14)70325-4

Jenkinson, M., Beckmann, C. F., Behrens, T. E. J., Woolrich, M. W., & Smith, S. M. (2012). FSL. *NeuroImage*, *62*(2), 782–790. https://doi.org/10.1016/j.neuroimage.2011.09.015

Jobst, B. C., & Cascino, G. D. (2015). Resective epilepsy surgery for drug-resistant focal epilepsy: A review. *JAMA - Journal of the American Medical Association*, *313*(3). https://doi.org/10.1001/jama.2014.17426

Koepp, M. J., Galovic, M., Baudracco, I., Wright-Goff, E., Pillajo, G., Nachev, P., Wandschneider, B., Woermann, F., Thompson, P., Baxendale, S., McEvoy, A. W., Nowell, M., Mancini, M., Vos, S. B., Winston, G. P., Sparks, R., Prados, F., Miserocchi, A., De Tisi, J., … Duncan, J. S. (2019). Association of piriform cortex resection with surgical outcomes in patients with temporal lobe epilepsy. *JAMA Neurology*, *76*(6). https://doi.org/10.1001/jamaneurol.2019.0204

Kuroda, N., Sonoda, M., Miyakoshi, M., Nariai, H., Jeong, J. W., Motoi, H., Luat, A. F., Sood, S., & Asano, E. (2021). Objective interictal electrophysiology biomarkers optimize prediction of epilepsy surgery outcome. *Brain Communications*, *3*(2). https://doi.org/10.1093/braincomms/fcab042

Leon-Rojas, J. E., Iqbal, S., Vos, S. B., Rodionov, R., Miserocchi, A., McEvoy, A. W., Vakharia, V. N., Mancini, L., Galovic, M., Sparks, R. E., Ourselin, S., Cardoso, J. M., Koepp, M. J., & Duncan, J. S. (2021). Resection of the piriform cortex for temporal lobe epilepsy: a Novel approach on imaging segmentation and surgical application. *British Journal of Neurosurgery*. https://doi.org/10.1080/02688697.2021.1966385

Löscher, W., Potschka, H., Sisodiya, S. M., & Vezzani, A. (2020). Drug resistance in epilepsy: Clinical impact, potential mechanisms, and new innovative treatment options. *Pharmacological Reviews*, *72*(3). https://doi.org/10.1124/pr.120.019539

Pérez-García, F., Rodionov, R., Alim-Marvasti, A., Sparks, R., Duncan, J. S., & Ourselin, S. (2020). Simulation of Brain Resection for Cavity Segmentation Using Self-supervised and Semi-supervised Learning. *Lecture Notes in Computer Science (Including Subseries Lecture Notes in Artificial Intelligence and Lecture Notes in Bioinformatics)*, *12263 LNCS*. https://doi.org/10.1007/978-3-030-59716-0_12

Ronneberger, O., Fischer, P., & Brox, T. (2015). U-Net: Convolutional Networks for Biomedical Image Segmentation. *Lecture Notes in Computer Science (Including Subseries Lecture Notes in Artificial Intelligence and Lecture Notes in Bioinformatics)*, *9351*, 234–241. https://doi.org/10.1007/978-3-319-24574-4_28

Yushkevich, P. A., Piven, J., Hazlett, H. C., Smith, R. G., Ho, S., Gee, J. C., & Gerig, G. (2006). User-guided 3D active contour segmentation of anatomical structures: Significantly improved efficiency and reliability. *NeuroImage*, *31*(3). https://doi.org/10.1016/j.neuroimage.2006.01.015